Adaptive Trajectory Tracking Control of Skid-Steered Mobile Robots

Jingang Yi
Dept. of Mech. Eng.
San Deigo State University
San Diego, CA 92182
jgyi@mail.sdsu.edu

Dezhen Song
Dept. of Computer Science
Texas A&M University
College Station, TX 77843
dzsong@cs.tamu.edu

Junjie Zhang
Dept. of Mech. Eng.
Texas A&M University
College Station, TX 77843
jjzhang@tamu.edu

Zane Goodwin
Dept. of Computer Science
Texas A&M University
College Station, TX 77843
zgoodwin@cs.tamu.edu

***Abstract*— Skid-steered mobile robots have been widely used for terrain exploration and navigation. In this paper, we present an adaptive trajectory control design for a skid-steered wheeled mobile robot. Kinematic and dynamic modeling of the robot is first presented. A pseudo-static friction model is used to capture the interaction between the wheels and the ground. An adaptive control algorithm is designed to simultaneously estimate the wheel/ground contact friction information and control the mobile robot to follow a desired trajectory. A Lyapunov-based convergence analysis of the controller and the estimation of the friction model parameter is presented. Simulation and preliminary experimental results based on a four-wheel robot prototype are demonstrated for the effectiveness and efficiency of the proposed modeling and control scheme.**

I. Introduction

Skid-steered mobile robots have been widely used in many applications, such as terrain navigation and exploration, waste management, defense, security, and household services. Figure 1 shows an example of a skid-steered four wheel mobile robot. The absence of a steering system of a skid-steered mobile robot (vehicle) makes the robot mechanically robust and simple for terrain or outdoor environment navigation. Due to the varying tire/ground interactions and over-constrained contact, it is quite challenging to obtain accurate dynamic models and tracking control systems for such mobile robots. Although there is a great deal of research on dynamic modeling and tracking control of differential-driven mobile robots that are under the nonholonomic constraint of zero lateral velocity, such as unicycles or car-like robots (readers can refer to [1] and references therein), the counterpart research on skid-steered mobile robots is less frequently reported.

Because of the similarity between skid-steering of tracked and wheeled vehicles, the method of modeling the track/ground interaction for tracked vehicles can be utilized for skid-steered wheeled robots. Song *et al.* [2] use the tracked vehicle models discussed in [3]. In [4], localization of a tracked vehicle based on kinematic models is presented. For skid-steered modeling of tracked vehicles, readers can refer to [5]–[7] for details. Because of the difficulty in accurately capturing skid-steering, Anousaki and Kyriakopoulos [8] propose an experimental study to model the kinematic relationship and demonstrate that a kinematic model for an ideal differential-driven wheeled robot cannot account for skid-steered robots.

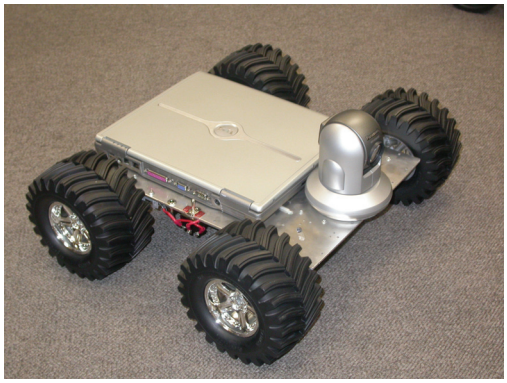

Fig. 1. A skid-steered four wheel mobile robot.

There is little work discussing the dynamic control of skid-steered mobile robots due to the lack of a good understanding of skid-steering and the complexity of the wheel/ground interactions. In [9], a dynamic model was presented for a skid-steered four-wheel robot and a nonholonomic constraint between the robot's lateral velocity and yaw rate is considered. A perfect knowledge of the wheel/ground contact was assumed. In [10], a simple Coulomb friction model is used to capture the wheel/ground interaction and a nonlinear feedback controller is designed to track the desired path. Ahmadi *et al.* [11] discuss tracked vehicle trajectory control and a linearized track-soil interaction model with known parameters is used for the controller design.

There are some research on modeling the wheel/ground interaction for mobile robots. In [12], a comparison study is presented for the control performance of an omni-directional mobile robot with and without considering wheel slip. It was found that the significance of slip increases when the wheel/ground friction coefficient is larger. A tire/road friction model in automotive study was considered for the longitudinal friction force in [12]. For a detailed review of the tire/road friction model, readers can refer to [13]. Dynamic modeling of wheel/ground interaction is also presented in [14] for wheeled omni-directional robots. The longitudinal and lateral friction coefficients are considered independently. Recently, Ray *et al.* [15] use the force-slip relationship from tire/road

interaction to control the slip for the cooperative control of a group of skid-steered autonomous mobile robots.

In this paper, a kinematic and dynamic model of the skid-steered four-wheel mobile robot is first presented to characterize the skid-steering properties. A wheel/ground friction model is incorporated into the robot model for both the longitudinal and lateral friction forces. Based on these models, an adaptive trajectory control algorithm is utilized to asymptotically track the desired trajectory. The contribution of this paper is twofold. First, we propose a dynamic model for skid-steered four-wheel mobile robots. Most existing work only discuss the kinematic model due to the complex dynamics involved in the wheel/ground interactions. Secondly, we propose an adaptive tracking control mechanism that could estimate the wheel/ground interaction in real time. Such a control system design can enhance the tracking control performance of a skid-steered mobile robot.

This paper is organized as follows. In section II, we discuss the kinematic and dynamic modeling of a four-wheel skid-steered mobile robot. A wheel/ground interaction model is also discussed in this section. Section III presents a trajectory control design for the skid-steered robot. Simulation and experimental results of a prototype robot are presented in section IV. Finally, we conclude the paper and discuss future research directions in section V.

II. Dynamic Models

Figure 2 shows the kinematic schematic of the skid-steered robot. Without loss of generality, we consider the following assumptions.

Assumption 1 *Robot modeling assumptions.*

1. *The mass center of the robot is located at the geometric center of the body frame* [1].
2. *There is point contact between the wheel and the ground.*
3. *The contact rolling resistance force is negligible* [2].
4. *Each side's two wheels rotate at the same speed.*
5. *The normal forces at the wheel/ground contact points are equally distributed among four wheels during motion.*
6. *The robot is running on a flat ground surface and four wheels are always in contact with the ground surface.*

Denote the wheel angular velocities ω_i and the velocities of the wheel contact points as v_i, $i = 1, \cdots, 4$, for the left-front, left-rear, right-front, and right-rear wheels, respectively. Assumption 1.4 implies $\omega_1 = \omega_2, \quad \omega_3 = \omega_4$. The longitudinal and lateral forces at each wheel's contact point are F_i and P_i, $i = 1, \cdots, 4$, respectively. The velocity of the robot mass center is denoted as v_G. We can define a fixed frame (X, Y) and a robot body frame (x, y) as shown in Fig. 2. We also denote the longitudinal and lateral wheel bases as L and W, respectively.

[1]Similar results could be obtained if the mass center of the robot were located somewhere other than the robot's geometric center.

[2]Since we only consider wheel/ground point contact, the ground resistance force is negligible.

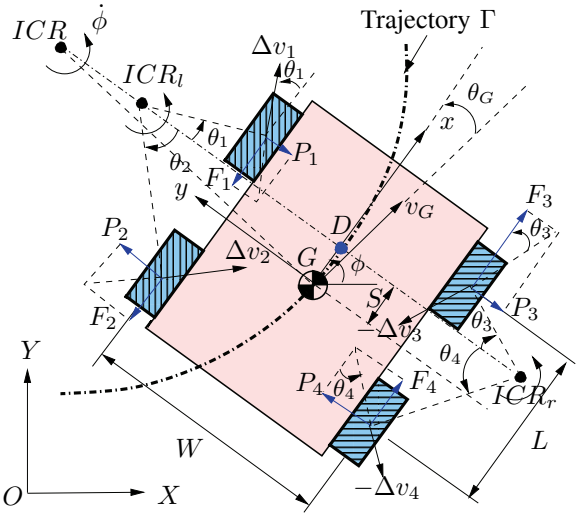

Fig. 2. A top-view schematic of the skid-steered mobile robot on a flat surface.

Because of Assumption 1.4, we denote the instantaneous center of rotation (ICR) of the left-side wheel contact points, right-side wheel contact points, and the robot body as ICR_l, ICR_l, and ICR_G, respectively. It is known that ICR_l, ICR_r and ICR_G lie on a line parallel to the x-axis [4], [7], [16]. Let $(\dot{x}, \dot{y}, \dot{\phi})$ be the longitudinal, lateral, and angular velocity of the robot in body frame (x, y). It is straightforward to calculate the relationship of the robot velocities and accelerations in both frames as follows.

$$\begin{bmatrix} \dot{X} \\ \dot{Y} \end{bmatrix} = \mathbf{R}^T(\phi) \begin{bmatrix} \dot{x} \\ \dot{y} \end{bmatrix}, \quad \begin{bmatrix} \ddot{X} \\ \ddot{Y} \end{bmatrix} = \mathbf{R}^T(\phi) \begin{bmatrix} \ddot{x} - \dot{y}\dot{\phi} \\ \ddot{y} + \dot{x}\dot{\phi} \end{bmatrix}, \quad (1)$$

where

$$\mathbf{R}(\phi) = \begin{bmatrix} \cos\phi & \sin\phi \\ -\sin\phi & \cos\phi \end{bmatrix}.$$

Given mass center velocity v_G and yaw rate $\dot{\phi}$, the longitudinal velocities v_{ix} of the wheel/ground contact points are

$$v_{1x} = v_{2x} = \dot{x} - \frac{W}{2}\dot{\phi}, \quad v_{3x} = v_{4x} = \dot{x} + \frac{W}{2}\dot{\phi}, \quad (2)$$

where r is the wheel radius. Then we can define the longitudinal wheel slips λ_i as

$$\lambda_i = \frac{r\omega_i - v_{ix}}{r\omega_i} = -\frac{\Delta v_{ix}}{r\omega_i}, \quad i = 1, \cdots, 4, \quad (3)$$

where $\Delta v_{ix} = v_{ix} - r\omega_i$. Note that $\lambda_1 = \lambda_2$ and $\lambda_3 = \lambda_4$ due to Assumption 1.4. It is also observed that under the above definition, $\lambda \in [0, 1]$ if the wheel is under traction, and $\lambda \in (-\infty, 0]$ if the wheel is under braking, which is undesirable for uniformly modeling the wheel/ground friction under traction and braking cases. To avoid such a problem, using the same treatment as in [5], we restrict the magnitude of λ to a maximum magnitude of 1.0 for $\lambda < 0$ under braking.

On the other hand, we denote the x-y coordinates for ICR_l, ICR_r, and ICR_G as (x_l, y_l), (x_r, y_r), and (x_G, y_G),

respectively. We can find that the x-coordinates S of the ICRs satisfies the following constraints [4], [16]

$$S = x_l = x_r = x_G = -\frac{\dot{y}}{\dot{\phi}}. \tag{4}$$

We can also write the longitudinal skid velocities of the wheel/ground contact points as[3]

$$\begin{aligned} \Delta v_{1x} = \Delta v_{2x} &= \left(y_l - \frac{W}{2}\right)\dot{\phi}, \\ \Delta v_{3x} = \Delta v_{4x} &= \left(y_r + \frac{W}{2}\right)\dot{\phi}. \end{aligned} \tag{5}$$

Combining Eqs. (2), (5), and $\Delta v_{ix} = r\omega_i - v_{ix}$, we can obtain

$$y_l = \frac{\dot{x} - r\omega_1}{\dot{\phi}}, \quad y_r = \frac{\dot{x} - r\omega_3}{\dot{\phi}}, \quad y_G = \frac{\dot{x}}{\dot{\phi}}. \tag{6}$$

We consider the longitudinal friction forces $F_i = N_i\mu_i$ for the ith wheel, where μ_i is the friction coefficient and N_i is the normal force. It has been widely considered that the friction coefficient μ is a function of the longitudinal slip λ [7], [13], [17]. Figure 3(a) shows the μ-λ curve that is obtained by fitting the experimental data [18]. Here, we consider a linear approximation of the μ-λ curve as shown in Fig. 3(b). For the traction case, the friction coefficient μ can be approximated by the following functions.

$$\mu(\lambda) = \begin{cases} K\lambda & \lambda \in [0, \lambda_m) \\ K\lambda_m - \frac{K\lambda_m - \mu_s}{1-\lambda_m}(\lambda - \lambda_m) & \lambda \in [\lambda_m, 1], \end{cases} \tag{7}$$

where K is the friction stiffness coefficient, λ_m is the longitudinal slip value which corresponds to the maximum wheel/ground friction coefficient, and μ_s is the longitudinal wheel/ground sliding friction coefficient.

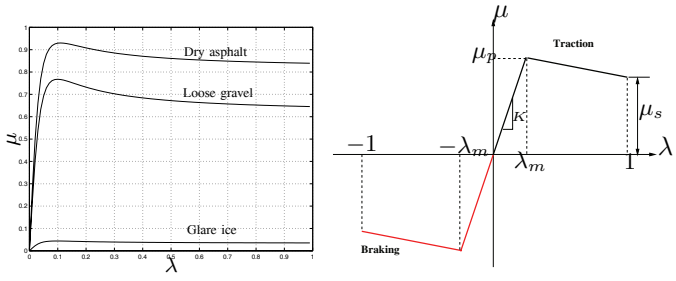

(a) (b)

Fig. 3. (a) Relationship between the wheel/ground friction coefficient μ and the longitudinal slip λ under various road conditions. (b) A linear approximation of the μ-λ relationship.

We assume that the sliding friction coefficient is a fraction of the peak friction coefficient μ_p, i.e. $\mu_s = \alpha\mu_p = \alpha K\lambda_m$, where $0 \le \alpha \le 1$. With such a simplification, we can rewrite Eq. (7) as

$$\mu(\lambda) = K\left[\sigma_1(\lambda) + \sigma_2(\lambda)\,\mathrm{sgn}(\lambda)\lambda\right], \tag{8}$$

[3]The IRCs are well-defined at a finite distance from the wheel/ground contact point for zero yaw rate $\dot{\phi} = 0$ since $\dot{y} = 0$ in this case [4].

where function $\mathrm{sgn}(x) = 1$ if $x \ge 0$ and $\mathrm{sgn}(x) = -1$ if $x < 0$ and

$$\sigma_1(\lambda) = \begin{cases} 0 & \text{if } 0 \le \lambda \le \lambda_m \\ \frac{1-\alpha\lambda_m}{1-\lambda_m}\lambda_m & \text{if } \lambda > \lambda_m, \end{cases}$$

and

$$\sigma_2(\lambda) = \begin{cases} 1 & \text{if } 0 \le \lambda \le \lambda_m \\ -\frac{1-\alpha}{1-\lambda_m}\lambda_m & \text{if } \lambda > \lambda_m. \end{cases} \tag{9}$$

Eq. (8) can still be used to calculate the *magnitude* of the friction coefficients for the braking case while the longitudinal slip $\lambda < 0$ and $\mu < 0$.

The longitudinal friction force F_i and the lateral friction P_i are dependent on each other and their magnitudes forms a friction force circle [16], [17], [19], namely, $F_i = F_{ir}\cos\theta_i$, $P_i = F_{ir}\sin\theta_i$, where F_{ir} is the resultant maximum friction force and θ_i is the slip angle at the ith wheel (see Fig. 2). Noting that the longitudinal friction force $F_i = N_i\mu_i(\lambda_i)$, then we can rewrite the lateral friction force P_i as

$$P_i = F_i\tan\theta_i, \quad i = 1, \cdots, 4, \tag{10}$$

where slip angles θ_i can be calculated as the angles between the line formed by the wheel contact point and the instantaneous rotating center and the centerline of the wheel's rotating axis (Fig. 2).

Figure 4 shows the four combinations of friction forces for each side of the wheels. The longitudinal forces F_i and the lateral forces P_i follow the relationship in Eq. (10). Denote the IRC coordinates as (x, y) and for all cases shown in Fig. 4 we can rewrite Eq. (10) as follows.

$$P_1 = F_1\,\mathrm{sgn}(\lambda_1)\frac{\frac{L}{2} - x}{y}, \; P_2 = -F_2\,\mathrm{sgn}(\lambda_2)\frac{\frac{L}{2} + x}{y}. \tag{11}$$

Notice that $y \ne 0$ and $F_1, F_2 \ge 0$ is the magnitude of the longitudinal friction force in the above equations.

For the four-wheel robot, we assume that the normal load at each wheel $N_i = \frac{mg}{4}$ is a constant and that the ground soil conditions are the same for the four wheels [4]. Due to the fact $\lambda_1 = \lambda_2$, $\lambda_3 = \lambda_4$, we can obtain $F_1 = F_2$, $F_3 = F_4$. Using the relationship given by Eq. (11), we can obtain

$$P_1 = F_1\,\mathrm{sgn}(\lambda_1)\frac{\frac{L}{2} - x_l}{y_l - \frac{W}{2}}, \; P_2 = -F_1\,\mathrm{sgn}(\lambda_1)\frac{\frac{L}{2} + x_l}{y_l - \frac{W}{2}}, \tag{12}$$

$$P_3 = F_3\,\mathrm{sgn}(\lambda_3)\frac{\frac{L}{2} - x_r}{-(y_r + \frac{W}{2})}, \; P_4 = -F_3\,\mathrm{sgn}(\lambda_3)\frac{\frac{L}{2} + x_r}{-(y_r + \frac{W}{2})}. \tag{13}$$

Therefore, we can write the dynamic equations in the (x, y) frame as follows.

$$m\ddot{x} = 2\left[\mathrm{sgn}(\lambda_1)F_1 + \mathrm{sgn}(\lambda_3)F_3\right] \tag{14a}$$

$$m\ddot{y} = P_1 + P_2 + P_3 + P_4 \tag{14b}$$

$$I_G\ddot{\phi} = 2\left[-\mathrm{sgn}(\lambda_1)F_1 + \mathrm{sgn}(\lambda_3)F_3\right]\frac{W}{2} - (-P_1 + P_2 - P_3 + P_4)\frac{L}{2}, \tag{14c}$$

[4]This is a reasonable assumption since the robot size is relatively small.

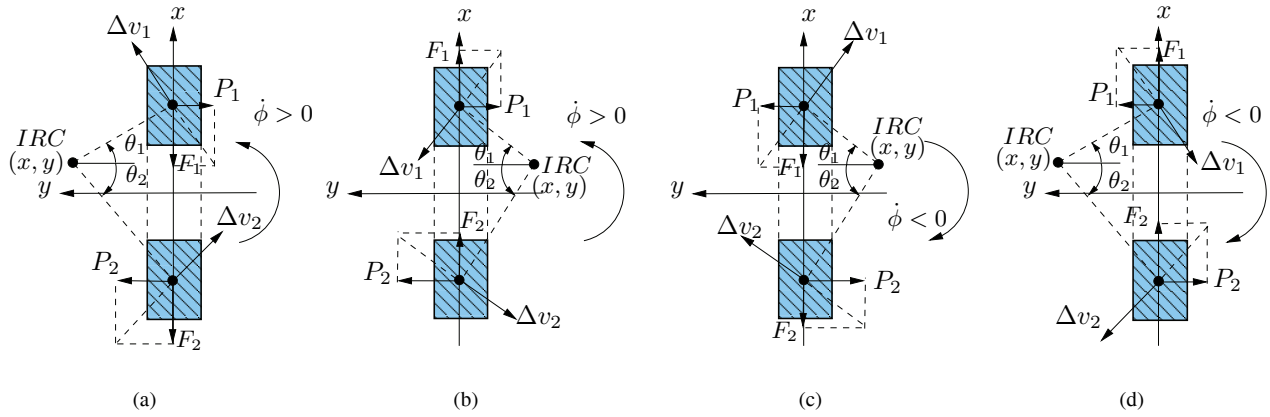

Fig. 4. Friction forces. (a) Braking while turning left, (b) traction while turning left, (c) braking while turning right, and (d) traction while turning right.

where m is the mass of the robot and I_G is the mass moment of inertia of the robot about its mass center G.

Using Eqs. (3), (5), (6), and (8), we can rewrite the traction/braking forces as

$$\begin{aligned} F_1 = F_2 &= \frac{mg}{4}K\sigma_1(\lambda_1) - \\ &\quad \frac{mg}{4}K\,\mathrm{sgn}(\lambda_1)\sigma_2(\lambda_1)\left[\left(\dot{x} - \frac{W}{2}\dot{\phi}\right)u_1 - 1\right] \\ F_3 = F_4 &= \frac{mg}{4}K\sigma_1(\lambda_3) - \\ &\quad \frac{mg}{4}K\,\mathrm{sgn}(\lambda_3)\sigma_2(\lambda_3)\left[\left(\dot{x} + \frac{W}{2}\dot{\phi}\right)u_2 - 1\right], \end{aligned} \tag{15}$$

where $u_1 = \frac{1}{r\omega_1}$ and $u_2 = \frac{1}{r\omega_3}$. Defining the control input variables $v_1 = \sigma_2(\lambda_1)u_1 - \sigma_2(\lambda_3)u_2$, $v_2 = \sigma_2(\lambda_1)u_1 + \sigma_2(\lambda_3)u_2$ and using the friction force model (15) and the relationship for λ_i, Eqs. (14a)-(14c) become

$$\ddot{x} = gK\left[\frac{1}{2}\sigma_\Sigma + \frac{1}{4}W\dot{\phi}v_1 - \frac{1}{2}\dot{x}v_2\right] \tag{16a}$$

$$\ddot{y} = -\frac{1}{2}gK\dot{y}\left[v_2\left(1 + \frac{1}{2}\sigma_{r1}\right) + \frac{1}{2}\sigma_{r2}v_1\right] \tag{16b}$$

$$\begin{aligned} \ddot{\phi} = \frac{mg}{4I_G}K\Big\{&-W\sigma_\Delta + \left(W\dot{x} + \frac{L^2}{2}\dot{\phi}\sigma_{r1}\right)v_1 - \\ &\frac{1}{2}\left[W^2 + L^2\left(1 + \frac{1}{2}\sigma_{r2}\right)\right]\dot{\phi}v_2\Big\}, \end{aligned} \tag{16c}$$

where

$$\sigma_{r1} = \frac{\sigma_1(\lambda_1)\,\mathrm{sgn}(\lambda_1\dot{\phi})}{\lambda_1\sigma_2(\lambda_1)} - \frac{\sigma_1(\lambda_3)\,\mathrm{sgn}(\lambda_3\dot{\phi})}{\lambda_3\sigma_2(\lambda_3)},$$
$$\sigma_{r2} = \frac{\sigma_1(\lambda_1)\,\mathrm{sgn}(\lambda_1\dot{\phi})}{\lambda_1\sigma_2(\lambda_1)} + \frac{\sigma_1(\lambda_3)\,\mathrm{sgn}(\lambda_3\dot{\phi})}{\lambda_3\sigma_2(\lambda_3)},$$

and $\sigma_\Sigma = \sigma_{1\Sigma} + \sigma_{2\Sigma}$, $\sigma_\Delta = \sigma_{1\Delta} + \sigma_{2\Delta}$, $\sigma_{1\Sigma} = \sigma_1(\lambda_1)\,\mathrm{sgn}(\lambda_1) + \sigma_1(\lambda_3)\,\mathrm{sgn}(\lambda_3)$, $\sigma_{1\Delta} = \sigma_1(\lambda_1)\,\mathrm{sgn}(\lambda_1) - \sigma_1(\lambda_3)\,\mathrm{sgn}(\lambda_3)$, $\sigma_{2\Sigma} = \sigma_2(\lambda_1) + \sigma_2(\lambda_3)$, and $\sigma_{2\Delta} = \sigma_2(\lambda_1) - \sigma_2(\lambda_3)$.

Defining the generalized coordinates $\mathbf{q} = [X\ Y\ \phi]^T$ and using Eq. (1), we can rewrite Eqs. (16) into the XY-frame as

$$\mathbf{M}\ddot{\mathbf{q}} + \mathbf{c}(\mathbf{q}, \dot{\mathbf{q}}) = \mathbf{E}(\mathbf{q}, \dot{\mathbf{q}})\mathbf{v}\,, \tag{17}$$

where $\mathbf{v} = [v_1\ v_2]^T$ and

$$\mathbf{M} = \begin{bmatrix} m & 0 & 0 \\ 0 & m & 0 \\ 0 & 0 & I_g \end{bmatrix}, \quad \mathbf{E}(\mathbf{q}, \dot{\mathbf{q}}) = \frac{1}{4}mgK\begin{bmatrix} \mathbf{R}^T\mathbf{E}_1 \\ \mathbf{e}_2 \end{bmatrix},$$

$$\mathbf{c}(\mathbf{q}, \dot{\mathbf{q}}) = m\dot{\phi}\begin{bmatrix} 0 & 1 & 0 \\ -1 & 0 & 0 \\ 0 & 0 & 0 \end{bmatrix}\dot{\mathbf{q}} - \frac{1}{4}mgK\begin{bmatrix} 2\mathbf{R}^T\begin{bmatrix}\sigma_\Sigma \\ 0\end{bmatrix} \\ -W\sigma_\Delta \end{bmatrix},$$

$$\mathbf{E}_1 = \begin{bmatrix} W\dot{\phi} & -2\dot{x} \\ \sigma_{r2}\dot{y} & -2\dot{y}\left(1 + \frac{1}{2}\sigma_{r1}\right) \end{bmatrix},$$

$$\mathbf{e}_2 = \begin{bmatrix} W\dot{x} + \frac{1}{2}L^2\sigma_{r1}\dot{\phi} & -\frac{\dot{\phi}}{2}\left[W^2 + L^2\left(1 + \frac{1}{2}\sigma_{r2}\right)\right] \end{bmatrix}.$$

We have to incorporate the nonholonomic constraint (4) into the above dynamics. Using Eq. (1), we can rewrite Eq. (4) as

$$\mathbf{A}(\mathbf{q})\dot{\mathbf{q}} = 0, \tag{18}$$

where $\mathbf{A}(\mathbf{q}) = [-\sin\phi \quad \cos\phi \quad S]$. Following a similar derivation in [9], we can find the following reduced state-space model [5]

$$\dot{\mathbf{q}} = \mathbf{G}(\mathbf{q})\boldsymbol{\eta} \tag{19a}$$

$$\dot{\boldsymbol{\eta}} = (\mathbf{G}^T(\mathbf{q})\mathbf{M}\mathbf{G}(\mathbf{q}))^{-1}\mathbf{G}^T(\mathbf{q})(\mathbf{E}\mathbf{v} - \mathbf{M}\dot{\mathbf{G}}(\mathbf{q})\boldsymbol{\eta} - \mathbf{c}), \tag{19b}$$

where $\boldsymbol{\eta} = [\eta_1\ \ \eta_2]^T = [\dot{x}\ \ \dot{y}]^T$ is the pseudo-velocity and matrix $\mathbf{G}(\mathbf{q})$ has its columns in the null space of $\mathbf{A}(\mathbf{q})$ [6].

$$\mathbf{G}(\mathbf{q}) = \begin{bmatrix} \cos\phi & -\sin\phi \\ \sin\phi & \cos\phi \\ 0 & -\frac{1}{S} \end{bmatrix} = \begin{bmatrix} \mathbf{R}^T \\ \mathbf{g}_1 \end{bmatrix}, \quad \mathbf{g}_1 = \begin{bmatrix} 0 & -\frac{1}{S} \end{bmatrix}.$$

We can simplify Eq. (19b) as follows.

$$\dot{\boldsymbol{\eta}} = \frac{mgK}{4}\mathbf{M}_\eta\left[\left(\mathbf{E}_1 + \mathbf{g}_1^T\mathbf{e}_2\right)\mathbf{v} + \begin{bmatrix} 2\sigma_\Sigma \\ \frac{W\sigma_\Delta}{S} \end{bmatrix}\right] \tag{20}$$

[5] We drop the variable dependency for those variables that have been previously defined.

[6] Here we can enforce $S \neq 0$ to define the matrices well. It is also observed in [4] that S is finite such that $\frac{1}{S} \neq 0$.

where

$$\mathbf{M}_\eta = \begin{bmatrix} \frac{1}{m} & 0 \\ 0 & \frac{1}{m+\frac{I_G}{S^2}} \end{bmatrix}.$$

III. Control System Design

Given the dynamic model of the skid-steered mobile robot (19a) and (20), we can design a dynamic feedback linearization based controller system [9]. We can first use the following input transformation for Eq. (20).

$$\mathbf{v} = \left(\mathbf{E}_1 + \mathbf{g}_1^T \mathbf{e}_2\right)^{-1} \left(\frac{4}{mg} \mathbf{M}_\eta^{-1} \boldsymbol{\tau} - \begin{bmatrix} 2\sigma_\sum \\ \frac{W\sigma_\Delta}{S} \end{bmatrix} \right), \tag{21}$$

where $\boldsymbol{\tau} = [\tau_1 \ \tau_2]^T$ is the new control input. Under such a transformation, Eq. (20) becomes

$$\begin{cases} \dot{\eta}_1 = K\tau_1 \\ \dot{\eta}_2 = K\tau_2. \end{cases}$$

Consider the new output function $\mathbf{z}(t)$ as the coordinates (in a fixed frame) of the IRC projection point on the x-axis (point D in Fig. 2).

$$\mathbf{z}(t) = \begin{bmatrix} X + S\cos\phi \\ Y + S\sin\phi \end{bmatrix}. \tag{22}$$

Defining $\tau_1 = \zeta$, $\dot{\zeta} = w_1$ (dynamic extension), $\tau_2 = w_2$, and $\mathbf{w} = [w_1 \ w_2]^T$, then we obtain

$$\ddot{\mathbf{z}} = K\boldsymbol{\alpha}(\mathbf{q}, \boldsymbol{\eta})\mathbf{w} + K\boldsymbol{\beta}(\mathbf{q}, \boldsymbol{\eta}) + \boldsymbol{\gamma}(\mathbf{q}, \boldsymbol{\eta}), \tag{23}$$

where

$$\boldsymbol{\alpha}(\mathbf{q}, \boldsymbol{\eta}) = \begin{bmatrix} \cos\phi & \frac{\eta_1}{S}\sin\phi \\ \sin\phi & -\frac{\eta_1}{S}\cos\phi \end{bmatrix}, \ \boldsymbol{\beta}(\mathbf{q}, \boldsymbol{\eta}) = \begin{bmatrix} \frac{2\zeta\eta_2}{S}\sin\phi \\ -\frac{2\zeta\eta_2}{S}\cos\phi \end{bmatrix},$$

and $\boldsymbol{\gamma}(\mathbf{q}, \boldsymbol{\eta}) = \begin{bmatrix} -\frac{\eta_1\eta_2^2}{S^2}\cos\phi & -\frac{\eta_1\eta_2^2}{S^2}\sin\phi \end{bmatrix}^T$. Let $\mathbf{z}_d(t)$ denote the desired trajectory of the mobile robot. Then we can define the tracking error $\boldsymbol{\epsilon} = \mathbf{z}(t) - \mathbf{z}_d(t)$ and the sliding surface $\mathbf{s}$ as $\mathbf{s} = \left(\frac{d}{dt} + a\right)^2 \boldsymbol{\epsilon} = \ddot{\boldsymbol{\epsilon}} + k_1\dot{\boldsymbol{\epsilon}} + k_2\boldsymbol{\epsilon}$, where $k_1 = 2a$, $k_2 = a^2$, and $a > 0$. Define $\theta = \frac{1}{K}$. From the friction model discussed in the previous section, we know that $0 < \theta < \infty$. Taking the time derivative of $\mathbf{s}$, we have

$$\dot{\mathbf{s}} = \dddot{\mathbf{z}} - \dddot{\mathbf{z}}_d + k_1\ddot{\boldsymbol{\epsilon}} + k_2\dot{\boldsymbol{\epsilon}}.$$

Using the dynamics given by Eq. (23), the above equation becomes

$$\dot{\mathbf{s}} = \frac{1}{\theta}\boldsymbol{\alpha}\mathbf{w} + \frac{1}{\theta}\boldsymbol{\beta} + \boldsymbol{\gamma} + \mathbf{f}(\mathbf{z}, \epsilon), \tag{24}$$

where $\mathbf{f}(\mathbf{z}, \epsilon) = -\dddot{\mathbf{z}}_d + k_1\ddot{\boldsymbol{\epsilon}} + k_2\dot{\boldsymbol{\epsilon}}$. Denote $\tilde{\theta} = \theta - \hat{\theta}$, where $\hat{\theta}$ is an estimate of the true parameter θ. We consider the following Lyapunov function candidate

$$V = \frac{1}{2}\mathbf{s}^T\mathbf{s} + \frac{1}{2\theta\rho}\tilde{\theta}^2,$$

where $\rho > 0$ is the adaptation gain. Let the control input $\mathbf{w}$ be

$$\mathbf{w} = \hat{\theta}\boldsymbol{\alpha}^{-1}\left(-\boldsymbol{\gamma} - \mathbf{f}(\mathbf{z}, \epsilon) - \xi\mathbf{s} - \frac{1}{\hat{\theta}}\boldsymbol{\beta}\right), \tag{25}$$

where $\mathbf{r} = -\boldsymbol{\gamma} - \mathbf{f}(\mathbf{z}, \epsilon) - \xi\mathbf{s}$ and $\xi > 0$ is a constant. Combining the above control design with Eq. (24) and taking the derivative of the Lyapunov function V, we have

$$\dot{V} = \mathbf{s}^T\dot{\mathbf{s}} + \frac{1}{\rho\theta}\tilde{\theta}\dot{\tilde{\theta}} = -\xi\mathbf{s}^T\mathbf{s} - \frac{\tilde{\theta}}{\theta}\left(\frac{\dot{\tilde{\theta}}}{\rho} + \mathbf{s}^T\mathbf{r}\right).$$

We can design the adaptation law for the estimation $\hat{\theta}$ as

$$\dot{\hat{\theta}} = -\rho\mathbf{s}^T\mathbf{r}. \tag{26}$$

Then the stability of the adaptive control system follows from $\dot{V} = -\xi\mathbf{s}^T\mathbf{s} \leq 0$ and Barbala's Lemma [20]. Note that the convergence of the estimated parameter $\hat{\theta}$ to its true value depends on the persistent excitation conditions for the adaptation law (26).

IV. Simulation and Experimental Results

In this section, we present some simulation and experimental results based on the skid-steered four-wheel robot platform shown in Fig. 1. For this robot, we have: $W = 0.43$ m, $L = 0.28$ m, $r = 0.08$ m, $m = 5$ kg, and $I_g = 0.45$ kgm^2.

Fig. 5 shows one test which compares the experiments with the simulation results. The robot was run under constant angular velocities $\omega_1 = \omega_2 = 60$ rpm and $\omega_3 = \omega_4 = 120$ rpm on a concrete surface. Fig. 5(a) shows the PID-controlled angular wheel speeds and Fig. 5(b) shows the real trajectory of the robot's center with a simulated circular trajectory under the same wheel speeds. Considering the mechanical alignment and geometric variations on the real system, the actual robot trajectory fits well with the simulated trajectory. A comparison of the results clearly shows that the dynamic model can predict the robot dynamics.

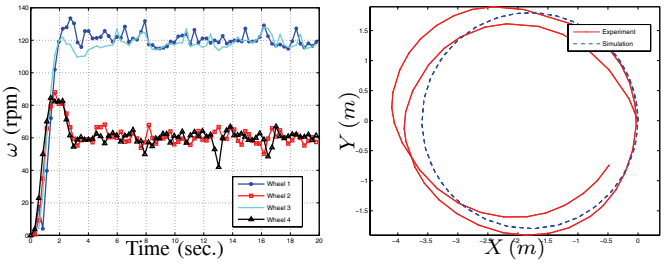

(a) (b)

Fig. 5. Experimental results for a circular motion with $\omega_1 = 60$ rpm and $\omega_3 = 120$ rpm. (a) Angular wheel speed, and (b) experimental and simulated trajectory.

In the simulation studying trajectory tracking control performance, the robot is designed to track a circle given by $x_d(t) = 6\sin\left(\frac{t}{10}\right)$ m and $y_d(t) = 6\cos\left(\frac{t}{10}\right)$ m. The location of the IRC of the robot is chosen as $S = 0.167$ m. For simplicity, the slope of the wheel/ground friction coefficient μ-λ curve is kept constant at $K = 5$ during the entire maneuver. The other parameters in the μ-λ curve are $\alpha = 0.8$ and $\lambda_m = 0.2$. The controller parameters are chosen as follows: $k_1 = 2$, $k_2 = 1$,

$\xi = 0.1$, and $\rho = 1$. The robot starts at location $(0, 3)$ with yaw angle $\phi(0) = 0$ and horizontal velocity $\dot{x} = 0.3$ m/s. The initial wheel velocities are $\omega_1(0) = \omega_2(0) = 20\pi$ rpm and the initial condition for the estimated parameter is $\hat{\theta}(0) = 1$. Figure 6(a) shows the robot trajectory, and Fig. 6(b) shows the tracking error in the fixed frame. It can be clearly seen from these plots that the robot trajectory quickly converges to the desired trajectory. Figure 7(a) shows the robot velocities in the body-fixed frame. It can be seen that since $S \neq 0$, the lateral velocity of the robot is non-zero, i.e. $\dot{y} \neq 0$, and the robot is indeed skidding on the ground. The estimated parameter $\hat{\theta}$ is shown in Fig. 7(b). Although the estimated parameter $\hat{\theta}$ converges, it does not converge to the true value $\theta = \frac{1}{K} = 0.2$.

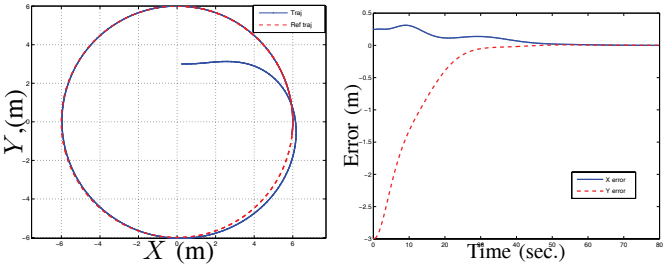

(a) (b)

Fig. 6. Simulation tracking results. (a) Robot trajectory, and (b) tracking error.

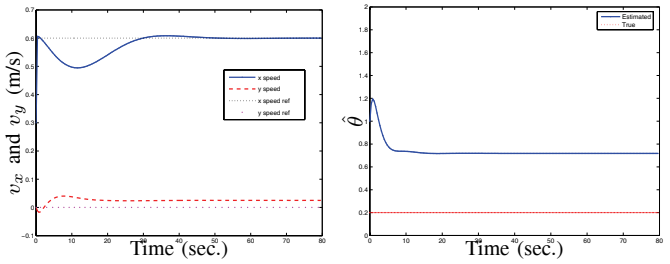

(a) (b)

Fig. 7. Simulation results. (a) Robot velocity in the body-fixed frame, and (b) the estimated friction parameter.

V. Conclusion

We presented an adaptive trajectory control design of a skid-steered wheeled mobile robot. An approximation of the wheel/ground friction forces was used to capture the dynamic relationship of the robot. The relationship between the longitudinal and lateral friction forces at each wheel was obtained through the rigid body kinematics of the robot frame and wheels at each side. An adaptive control algorithm was designed to simultaneously estimate the wheel/ground contact friction information and control the mobile robot to follow a desired trajectory. The stability of the adaptive controller was guaranteed by a Lyapunov stability analysis. However, the convergence of the estimated friction parameter to its true value depends on the richness of the adaptation signals. Some experimental and simulation results were presented to demonstrate the effectiveness and efficiency of the proposed modeling and control scheme.

In the future, we will report the experimental testing results of the proposed control mechanism on various road conditions. Additionally, some special maneuvers will be designed to create the persistent excitation conditions to precisely estimate the wheel/ground friction properties in real time.

References

[1] G. Oriolo, A. De Luca, and M. Vendittelli, "WMR Control Via Dynamic Feedback Linearization: Design, Implementation, and Experimental Validation," *IEEE Trans. Contr. Syst. Technol.*, vol. 10, no. 6, pp. 835–852, 2002.

[2] Z. Song, Y. Zweiri, and L. Seneviratne, "Nonlinear Observer for Slip Estimation of Skid-Steering Vehicles," in *Proc. IEEE Int. Conf. Robotics Automation*, Orlando, FL, 2006, pp. 1499–1504.

[3] A. Le, D. Rye, and H. Durrant-Whyte, "Estimation of Track-Soil Interactions for Autonomous Tracked Vehicles," in *Proc. IEEE Int. Conf. Robotics Automation*, Albuquerque, NM, 1997, pp. 1388–1393.

[4] J. Martinez, A. Mandow, J. Morales, S. Pedraza, and A. Garcia-Cerezo, "Approximating Kinematics for Tracked Mobile Robots," *Int. J. Robot. Res.*, vol. 24, no. 10, pp. 867–878, 2005.

[5] M. Kitano and M. Kuma, "An Analysis of Horizontal Plane Motion of Tracked Vehicles," *J. Terramechanics*, vol. 14, no. 4, pp. 211–225, 1977.

[6] J. Wong, *Theory of Ground Vehicles*, 3rd ed. Hoboken, NJ: John Wiley & Sons, Inc., 2001.

[7] J. Wong and C. Chiang, "A General Theory for Skid Steering of Tracked Vehicles on Firm Ground," *Proc. Inst. Mech. Eng., Part D: J. Auto. Eng.*, vol. 215, pp. 343–355, 2001.

[8] G. Anousaki and K. Kyriakopoulos, "A Dead-Reckoning Scheme for Skid-Steered Vehicles in Outdoor Environments," in *Proc. IEEE Int. Conf. Robotics Automation*, New Orleans, LA, 2004, pp. 580–585.

[9] L. Caracciolo, A. De Luca, and S. Iannitti, "Trajectory Tracking Control of a Four-Wheel Differentially Driven Mobile Robot," in *Proc. IEEE Int. Conf. Robotics Automation*, Detroit, MI, 1999, pp. 2632–2638.

[10] P. Petrov, J. de Lafontaine, P. Bigras, and M. Tetreault, "Lateral Control a Skid-Steering Mining Vehicle," in *Proc. IEEE/RSJ Int. Conf. Intel. Robots and Systems*, Takamatsu, Japan, 2000, pp. 1804–1809.

[11] M. Ahmadi, V. Polotski, and R. Hurteau, "Path Tracking Control of Tracked Vehicles," in *Proc. IEEE Int. Conf. Robotics Automation*, San Francisco, CA, 2000, pp. 2938–2943.

[12] R. Balakrishna and A. Ghosal, "Modeling of Slip for Wheeled Mobile Robots," *IEEE Trans. Robot. Automat.*, vol. 11, no. 1, pp. 126–132, 1995.

[13] J. Yi, "A Fault Tolerant Longitudinal Control and Tire/Road Friction Estimation System for Automated Highway Systems (AHS)," Ph.D. dissertation, Dept. Mech. Eng., Univ. Calif., Berkeley, 2002.

[14] R. L. Williams, II, B. E. Carter, P. Gallina, and G. Rosati, "Dynamic Model with Slip for Wheeled Omnidirectional Robots," *IEEE Trans. Robot. Automat.*, vol. 18, no. 3, pp. 285–293, 2002.

[15] L. Ray, D. Brande, J. Murphy, and J. Joslin, "Cooperative Control of Autonomous Mobile Robots in Unknown Terrain," in *Proc. ASME Int. Mech. Eng. Cong. Expo.*, Chicago, IL, 2006, IMECE2006-13435.

[16] K. Weiss, "Skid-Steering," *Auto. Eng.*, pp. 22–25, 1971.

[17] U. Kiencke and L. Nielsen, *Automotive Control Systems*. Berlin, Germany: Springer-Verlag, 2000.

[18] J. Yi, L. Alvarez, and R. Horowitz, "Adaptive Emergency Brake Control with Underestimation of Friction Coefficient," *IEEE Trans. Contr. Syst. Technol.*, vol. 10, no. 3, pp. 381–392, 2002.

[19] X. Claeys, J. Yi, R. Horowitz, C. Canudas de Wit, and L. Richard, "A New 3D Tire/road Friction Model for Vehicle Simulation," in *Proc. ASME Int. Mech. Eng. Cong. Expo.*, New York, NY, 2001, IMECE2001/DSC-24528.

[20] H. Khalil, *Nonlinear Systems*, 2nd ed. NJ: Prentice Hall, 1996.